Available online at www.sciencedirect.com
SCIENCE DIRECT®
Polymer 44 (2003) 6599–6606
polymer
www.elsevier.com/locate/polymer

Nanoscale mechanical properties of polymers irradiated by UV

Marek Nowicki[a,*], Asta Richter[b], Bodo Wolf[b], Halina Kaczmarek[c]

[a]*Institute of Physics, Poznań University of Technology, Ul. Nieszawska 13A, 60-965 Poznań, Poland*
[b]*Department of Engineering Science, University of Applied Science, Bahnhofstrasse 1, 15745 Wildau, Germany*
[c]*Faculty of Chemistry, Nicolaus Copernicus University, Gagarina 7, 87-100 Toruń, Poland*

Received 23 June 2003; received in revised form 16 July 2003; accepted 1 August 2003

Abstract

The application of depth sensing nanoindentation to determine mechanical properties of three different polymers is described in this work using three different techniques to calibrate the measurement system. The nano-hardness and the elastic indentation modulus of polyvinyl chloride, polyethylene oxide and polyacrylic acid were inferred from nanomechanical tests, and the influence of ultraviolet irradiation on the mechanical properties of measured polymers is studied. A multicycling test—a sequence of several loading and unloading procedures—allowed the measurement of changes in the sample viscoelasticity. The nano-hardness of the polymers is shown to increase with radiation dose while the viscoelasticity decreases.

Keywords: Scanning force microscopy; Nanoindentation; Polymers

1. Introduction

Scanning force microscopy (SFM), developed by G. Binnig and H. Rohrer [1,2], permits surface imaging of a broad scale of materials with nanometer resolution. This technique is also suitable for surface characterisation of organic materials [3,4]. On the contrary to other methods such as scanning tunnelling microscopy and transmission electron microscopy, it does not require any special preparation of the sample. One of the latest extensions of this technique is the nanoindenting SFM (NI-SFM) [5–8]. The HYSITRON-system, the first commercial representative of nanomechanical test equipment of this type, takes advantage of an electrostatic transducer to obtain the topography of the sample surface by SFM in contact mode. Moreover, it is possible to investigate the local mechanical properties of samples [9,10] at any selected point. This technique has been successfully used for the study of various nanomechanical properties of polymer single crystals and amorphous polymer thin films, including elasticity [11,12], hardness [13] and viscoelasticity measurements [14,15]. Depth sensing nanoindentation differs from classical hardness measurements (Vickers, Brinell and Knoop), where the impressions are first generated, and then imaged using a microscopy technique. Load and penetration depth are simultaneously recorded during both loading and unloading, resulting in a force–depth diagram. This diagram provides much more information than a microscopy image of the impression since it tells us the 'story' of the elastic and plastic deformation with increasing load (Fig. 1) and permits the determination of hardness and the elastic indentation modulus as a function of penetration depth. Moreover, the hardness measurements can be made with penetrations smaller than 1 μm. This offers possibilities to study the mechanical properties of the outermost layer of a polymer which is extremely susceptible to destruction under UV radiation.

The chemical structure of polymers has a strong influence on physical and mechanical properties of plastics [16,17]. Moreover, the mechanical properties of polymers change due to the influence of various environmental factors. Ultraviolet (UV) irradiation is one of the most destructive factors and it involves formation of radicals in macro-chains followed by a breakdown of chemical bonds [17,18]. The most significant reactions occurring in a polymer upon its exposure to UV irradiation are main chain scission, oxidation, side groups abstraction, or destruction [18–21]. Since the photodegradation of solid polymers starts in a very thin surface layer, it is very important to use

* Corresponding author. Tel.: +48-613-565-609; fax: +48-616-653-201.
E-mail address: mnowicki@phys.put.poznan.pl (M. Nowicki).

0032-3861/$ - see front matter © 2003 Published by Elsevier Ltd.
doi:10.1016/S0032-3861(03)00729-8

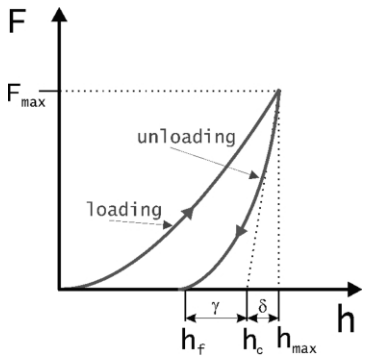

Fig. 1. Schematic representation of the force–depth curve for a nanoindentation procedure. The symbol, γ represents the plastic deformation part, and δ the elastic deformation part of the indent.

such a technique, which enables us to monitor changes of mechanical properties within a surface layer thinner than 1 μm. Depth sensing nanoindentation was found to be best suited for this aim [6,7]. The focus of this work is to study the changes of nano-hardness and mechanical properties of polymers upon UV irradiation.

Three commercial polymers with different chemical structure (Scheme 1) and different physical properties were selected for these investigations. All tested polymers find a broad application in many branches of industry and in daily life as well.

2. Experimental part

2.1. Sample preparation

Polyvinylchloride (PVC) from Polanvil S-67S, Anvil, Włocławek, Poland, polyethylene oxide (PEO) from Union Carbide, USA and polyacrylic acid (PAA) prepared in our laboratory by polymerisation in aqueous solution at 70 °C using 30% hydrogen peroxide as initiator, were used without addional purification. Thin solid films of PVC, PAA and PEO were prepared by pouring of solutions onto a glass plate and subsequent solvent evaporation. The film thickness was about 10–50 μm. All polymeric films were then UV-irradiated using a low-pressure mercury lamp (TUV30W, Philips, Netherlands) under ambient conditions. The main wavelength of UV-radiation was 254 nm. The

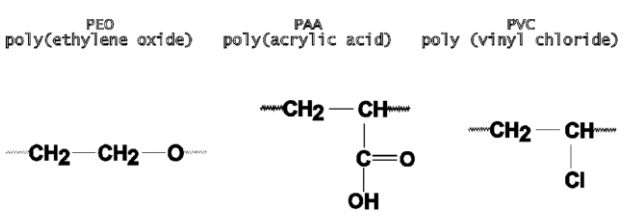

Scheme 1. Chemical structure of the studied polymers PEO, PAA and PVC.

intensity of incident light measured by the radiometer IL 1400A (International Light, USA), was 4.5 mW/cm^2.

2.2. Experimental equipment

All experiments were performed using a Hysitron TriboScope (electrostatic transducer) attached to a scanning force microscope with a controller Nanoscope E of the Veeco Metrology Group. The tip is made of diamond having the shape of a cube corner (three-sided pyramid). They were carried out at room temperature in air atmosphere. The following parameters were obtained (Fig. 1): maximum indentation depth (h_{max}), contact depth (h_c), depth of the remaining impression after complete unloading (h_f), maximal applied force (F_{max}), nano-hardness and Young's indentation modulus. The measurements were repeated a minimum of 5–10 times for all samples, and the average value was calculated.

The key quantities to determine the mechanical properties are defined as follows. The maximum indentation depth h_{max} includes elastic and plastic deformation. The depth at which the applied forces becomes zero on unloading is called h_f. The depth h_c is the contact depth at which the cross section area A_c is taken to calculate hardness and indentation modulus. The nano-hardness of the sample (H_N) is determined using the formula:

$$H_N = \frac{F_{max}}{A_c h_c}, \tag{1}$$

where F_{max} is the maximum applied load and A_c is the cross-sectional area corresponding to the depth h_c (see Fig. 1). The determination of the contact depth h_c is given by Ref. [22]

$$h_c = h_{max} - 0.75\frac{F_{max}}{S}, \tag{2}$$

where S is the contact stiffness

$$S = \frac{dF}{dh}, \tag{3}$$

with dF/dh being the slope of the unloading curve at the initial point of unloading. The reduced Young's indentation modulus E_r is a measure of the elastic properties of the tip-sample system and can be calculated from the load-depth curves according to the formula

$$E_r = \frac{1}{2}\sqrt{\frac{\pi}{A_c(h_c)}}\frac{dF}{dh} \tag{4}$$

For elastically deformable indenters, the reduced modulus E_r can be generalised and is defined as

$$\frac{1}{E_r} = \frac{1-\nu_s^2}{E_s} + \frac{1-\nu_t^2}{E_t} \tag{5}$$

where E_s and ν_s are the indentation modulus and Poisson ratio of the sample, E_t and ν_t are the indentation modulus and Poisson ratio of the indenter tip. Since E_t is much higher than E_s the value of E_r will hardly differ from E_s.

2.3. Calibration of the nanoindenter

The most important part of the Nanoindenter is the electrostatic transducer (three-plate capacitor). It enables both imaging of the sample surface (for topography information) and indenting. During the indenting process two types of data are stored simultaneously: the applied force and the indentation depth.

For a tip of ideal cube corner pyramid geometry the relation between indentation depth (h) and cross section area (tip area function A_c) is

$$A_c = 2.598h^2$$

The tip does not have an ideal shape but is blunted due to micromechanical generation of the tip shape and the use for imprinting into a material. A typical value of the blunting radius of the tip is 100 nm, and—though the tip is made of diamond—the radius of curvature will increase during frequent use. Thus, the determination of the real relation $A_c(h)$ is necessary for proper calculation of nano-hardness and Young's indentation modulus, particular in case of small penetrations. Three different methods to obtain this relation have been used and will be described in the following.

2.3.1. Tip imaging using a grid of sharp cones

In case of scanning of very sharp elements by a relatively blunt tip, there occurs the so-called 'opposite imaging'. When the element, protruding from the sample surface, has a significantly larger aspect ratio (quotient between height and lateral dimension) than the tip, the resulting image is in fact that of the tip. This is shown in Fig. 2. The effect of opposite imaging has been used as the first method to calculate the tip area function $A_c(h)$. We used a commercial grid with ultra sharp conical silicon tips TGZ 02 The distribution and the shape of the grid tips is shown in Fig. 3.

The small apex angle of the tips (below 20°) together with their large height (700 nm) offer possibilities for exact examination of the shape of the indentation diamond. Fig. 3 compares a Scanning Electron Microscopy image of the used grid with the SFM height topography image obtained by scanning the indentation diamond tip over the grid.

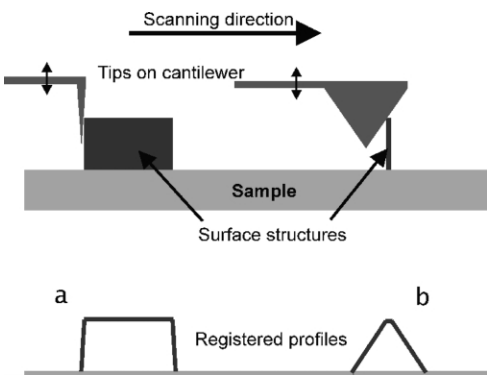

Fig. 2. Examples of overlapping profiles of tip and surface in the image pattern. (a) Sharp tip and bulky surface pattern, (b) bulky tip and sharp surface pattern.

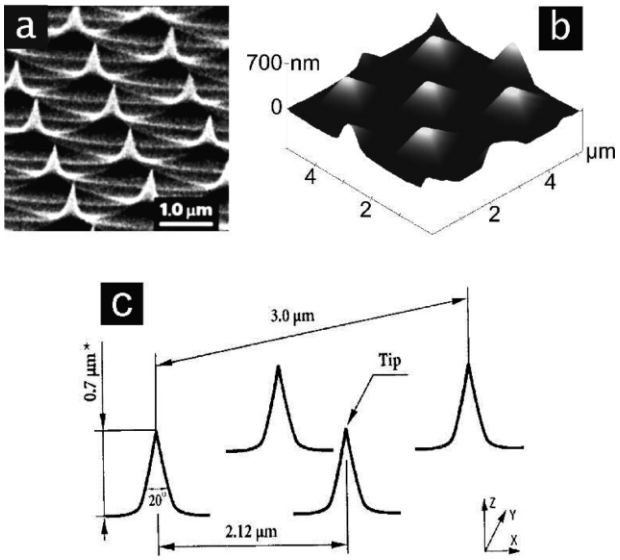

Fig. 3. Original silicon calibration grid TGZ 02 with ultra sharp tips, (a) scanning electron microscopy image and (c) schematic view of the arrangement of the tips with a tip radius less than 10 nm and a high aspect ratio; (b) SFM image of the calibration grid scanned with the diamond tip used for nanoindentation.

By means of the SFM software (using the so-called bearing function) the shape of the indenter diamond can be reconstructed (Fig. 3(b)) and the area function A_c can be obtained (Fig. 4). The advantage of this technique is the direct observation of the tip shape, which also allow to see the tip damage as outbreaks. It proves, however, very time-consuming. Furthermore, the deconvolution with the shape of the cone which was used for imaging is required. Therefore, a calibration procedure, better suited for every day practice, is described in the following section.

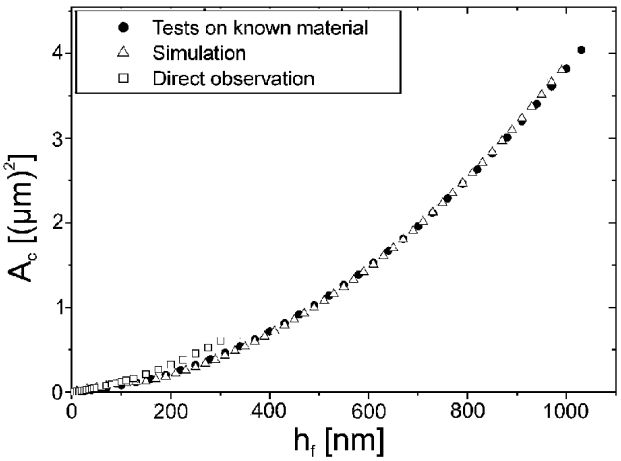

Fig. 4. Area functions obtained with three calibration procedures: circles—standard method with indents into fused silica with known material parameters; triangles—simulation of tip radius and corner angle measurement; squares—volume and area reconstruction from SFM-imaging of the grid of Fig. 3.

2.3.2. Tip calibration

To calibrate the tip, a series of indentations of different loads and depths into a specimen of known mechanical properties was performed. Then the area A_c as a function of depth can be determined such that the correct values of the sample are obtained. Since hardness is a quantity that depends on real structure of the material and is normally subject to an indentation size effect, this entity is not suited for calibration. Better suited is the elastic modulus which is hardly influenced by nanoscopic defects and should be constant. The test specimen should be homogeneous and isotropic, and should not be subject to chemical alterations, i.e. oxidation. A suited material is fused quartz, which also gives a large elastic re-deformation on unloading (very ductile materials with a small contribution of the elastic deformation to the total penetration, as copper, e.g. are not suited for this purpose). A series of 50 tests was made on fused quartz with the following parameters:

Young's modulus $E_0 = 72$ GPa
Poisson' number $\nu_0 = 0.17$.

This results in 50 data pairs $(h_i, A_c(h_i))$, $i = 1, \ldots, 50$

The data can then be fitted to any suitable function. This function should include a parabolic term (representing the ideal pyramid), a linear term (representing a spherical blunting) and other terms characterising tip truncation. We used an expression [22]

$$A_c = a_0h^2 + a_1h + a_2h^{1/2} + a_3h^{1/4} + a_4h^{1/8} + a_5h^{1/16}$$

and determined following coefficients:

$$A_c = 3.39h^2 + 4.09 \times 10^2h - 4.89 \times 10^2h^{1/2} + 0 \times 10^6h^{1/4} + 0 \times 10^5h^{1/8} + 1.80 \times 10^3h^{1/16}$$

This area function is shown as black circles in Fig. 4.

The tip can also be simulated as combination of a sphere added to the trunk of a cube corner pyramid [23,24]. It has been assumed that the very end of the tip is a sphere with the radius of 0.21 μm (as obtained from tip shape reconstruction using the AFM image of the silicon grid) which at a depth of 0.15 μm starts gradually to turn into the shape of the pyramid. The area function for this body is shown as white squares in Fig. 4. All three models deliver almost identical area functions.

3. Results and discussion

3.1. Measurements of nano-hardness and Young's indentation modulus of polymers

After calibration of the nanoindenter, measurements on polymer samples were performed. The force–depth curves (Fig. 5) shows a typical remaining plastic deformation of the polymer material during indentation of the tip. Increasing the load to its maximum value causes an elastic and plastic deformation of the material. The load is decreased to zero and the indentation depth is reduced to h_f. In all three investigated materials the final indentation depth at zero force h_f with 400 nm for PEO, 550 nm for PVC and 360 nm for PAA indicates that PEO is softer than PVC, and PAA is the hardest material. The corresponding hardness values for these materials calculated with a standard procedure using formula (1) and (2) are 0.13 GPa for PEO, 0.41 GPa for PVC and 0.77 GPa for PAA.

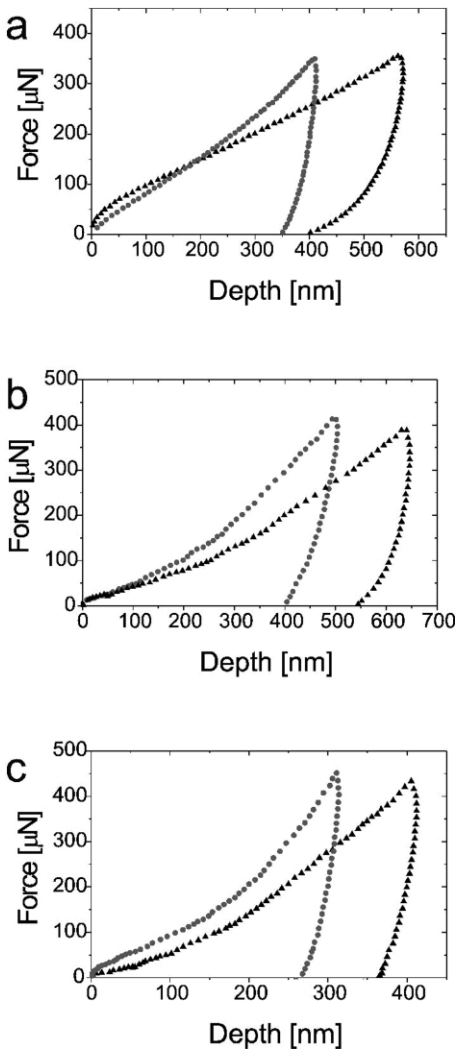

Fig. 5. Typical force–depth curves for (a) PEO, (b) for PVC and (c) PAA before (triangles) and after 10 h (circles) UV irradiation.

Macroscopic investigations of polymer materials rely on different measuring procedures. The Shore hardness for PAA is between 40 and 90 [25] which can be related to our hardness value of 0.77 GPa after transformation of standard engineering values to SCSI units with GPa. For PVC we found a Rockwell R 98 value of 1.06 [26], which is larger than our measured value. The indentation modulus also differs from the tensile strength value for macroscopic investigations, which is found to be between 6.9 and

11.7 GPa for PAA and 0.3–3.1 GPa for PVC. For PEO, the Young's modulus values vary between 0.2 and 5 GPa [27].

The morphology of the polymers investigated by macsoscopic methods in other groups are not completely comparable with our own polymer samples and depend on many additional parameters. Moreover, it is not possible to compare the indentation results directly with macroscopic investigations where the methods and the tested volumes are completely different. We mainly use the nanoindentation measurements for a relative comparison of the materials and the changes caused by UV irradiation.

UV irradiation causes in all three investigated polymers a hardening. This means that the maximum indentation depth and the remaining final indentation depth are smaller than in the non-irradiated material (see Fig. 5). The loading curve is also steeper in comparison to the non-irradiated polymers. A detailed description of the changes in E_{red} and H_N in dependence on UV irradiation is given in Fig. 7. The hardening process by UV irradiation is largest for PEO. After 10 h UV irradiation the polymer is about six times harder than the non-irradiated material. Simultaneously the elastic indentation modulus E_{red} increases by a factor of about 2.5. PVC shows only a minor reaction to UV irradiation during this time period of 10 h. After an extension of the UV exposure time up to 30 h a hardness increase by a factor of 1.85 is observed whereas the elastic indentation modulus is almost constant. The response time to UV irradiation in PAA is faster than in PVC, however, does not reach the significance as in PEO. Both the hardness and the indentation modulus in PAA increase by a factor of about 1.5 after 8 h UV exposure time.

There is a certain scattering of the measured values for the reduced elastic modulus E_{red} and the nano-hardness H_N (see Fig. 6), which is larger for smaller indentation depths. The typical scattering of hardness and elastic data was about maximum 20% (Fig. 6), mainly caused by surface roughness and lack of sample homogeneity. The surface irregularities of the polymer samples under study are difficult to avoid when using the mentioned method of sample production, which also applies to the lack of sample homogeneity. At the surface, the layer is mainly composed of oligomers, that can have different mechanical properties in comparison to the more homogenous sample interior of the polymer film. However, this effect is probably less significant than surface roughness. Considering the data scatter for small penetrations, it is necessary to conduct tests for which the contact depth is larger than about 300 nm.

Measured values of indentation modulus and nano-hardness as a function of UV exposure time are shown in Fig. 7. For all samples, UV irradiation results in an increase

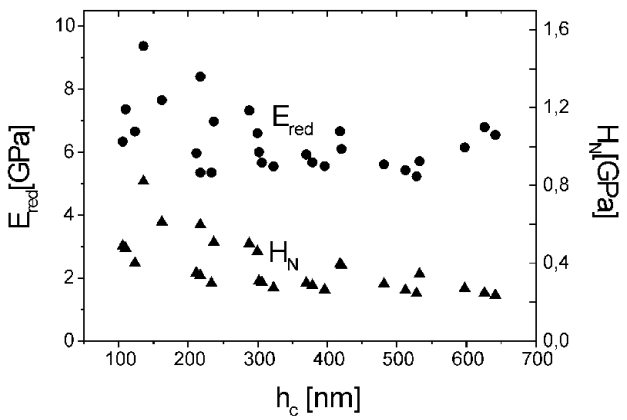

Fig. 6. Data scatter of reduced indentation modulus (circles) and nano-hardness (triangles) as a function of contact depth for irradiated PEO.

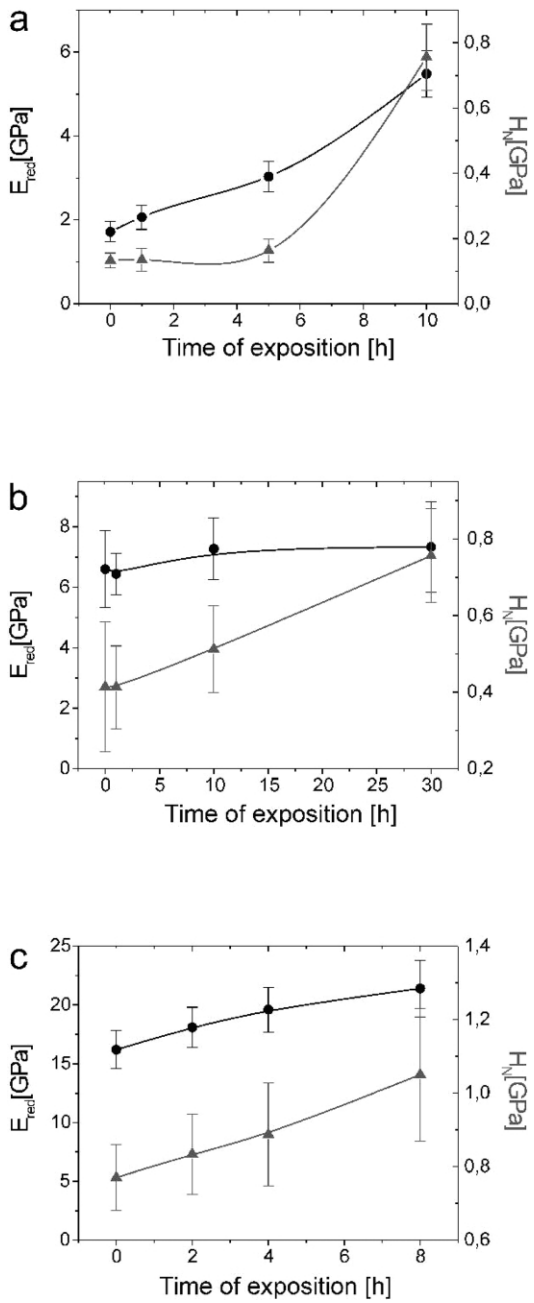

Fig. 7. Values of reduced indentation modulus and nano-hardness as a function of UV exposure time for PEO (a), PVC (b), PAA (c). The error bars quantify the scattering of the values by use of the standard deviation.

of E_{red} and H_N. Each sample was tested minimum ten times, using a multicycling load-depth regime with loads ranging between 20 and 500 μN. A set of values for the indentation modulus and the nano-hardness is obtained. Their statistical standard deviation was calculated. The error bars in Fig. 7 indicate the scattering of the values for the reduced elastic modulus E_{red} and the nano-hardness H_N and represent the statistical standard deviation for several measuring points along the surface. The statistical standard deviation varies due to inhomogeneities in the polymer matrix as for example shown for PEO surfaces in Fig. 8. The deviation is fairly small for the non-irradiated material or that with a small exposure time for UV irradiation. The reduced elastic modulus E_{red} has a larger deviation width after 5 and 10 h UV irradiation due to the crystalline areas shown in Fig. 8. This is also reflected in the nano-hardness H_N. It seems that the deviation width for all samples increases with increasing UV exposure time, except for the case of the non-irradiated PVC sample. This gives a hint of the hardening mechanism.

However, the trend of these changes in the reduced elastic indentation modulus E_{red} and nano-hardness H_N is different in various polymers, caused by the different course of photochemical reactions in the polymers studied. For PEO, only unimportant hardness changes were observed after the first 5 h of irradiation. After longer irradiation, the hardness increases starts to accelerate. Simultaneously, E_{red} increases slowly but systematically in this polymer for the whole irradiation period. In PVC, E_{red} vs. irradiation time is more linear than for PEO, and the changes of H_N are more significant. However, the hardness of UV-irradiated PVC changes less than it was found in PEO. For PAA, both parameters E_{red} and H_N increase gradually (nearly linearly) during the measured range of exposition time.

Different characteristics of mechanical parameters in our polymers during their UV irradiation can be caused by competitive reactions occurring with different efficiency. All polymers were studied at temperatures below their glass transition. As can be seen, PAA is the hardest and most mechanically resistant material among these three polymers. The most significant increase of H_N and E_{red} after UV irradiation was found for PEO, which has the lowest indentation modulus and the lowest hardness of the three investigated polymers. However, only PEO is highly crystalline, in contrast to PAA and PVC which are mainly amorphous. All polymers undergo photochemical reactions, but their sensitivity to UV irradiation is different. Moreover, the mechanisms of these phototransformations are dependent on the chemical structure of the polymer.

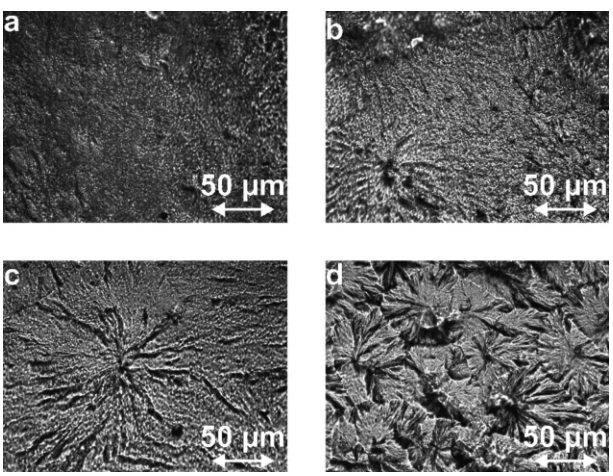

Fig. 8. Optical microscopy observations of the PEO surface for samples with different UV irradiation time: (a) non-irradiated, irradiation of (b) 1 h, (c) 5 h and (d) 10 h.

The polymer photodegradation is initiated when a macromolecule is excited by UV absorption. When the polymer has no absorbing groups in its units, impurities or structural defects can act as photoinitiators [28,29]. The excitation energy may be transferred to 'weak bonds' which can easily break down.

The principle reaction occurring in UV-irradiated polymers is the main-chain scission or side-group abstraction (Scheme 2). Reaction (A) leading to significant shortening of chain length, causes the deterioration of mechanical properties and the decrease of hardness. Degradation products of low molecular weight, present in UV-irradiated samples, plasticize the polymer and additionally reduce its hardness. The competitive reaction is photo-crosslinking, which is thought to cause the increase of Young's indentation modulus and hardness of the polymer [30,31]. The small increase of E and H observed in PAA and PVC clearly indicates that the photo-crosslinking is the dominant reaction in these polymers.

The increase of H_N and E_{red} in PEO cannot be explained by crosslinking [32], because it does not undergo such a reaction during UV exposure, and insoluble gel is not formed. PEO is known as a very unstable polymer. Its photodegradation occurs with high efficiency in the amorphous phase, whereas the crystalline part behaves relatively photoresistant. During photodegradation, the amorphous part is removed in the form of volatile products, and the remaining crystallites are characterised by high H- and E-values [33]. Furthermore, it seems to be possible that some rearrangement of shorter degraded chains occurs in the PEO surface, which can improve macromolecule order and increases the degree of crystallinity (see also the force–depth curves for small depths up to 200 nm in Fig. 5(a)).

3.2. Observation of the PEO surface by light microscopy

Microscopic observation confirms the previous model that UV-treatment of PEO leads to reorganisation of the macromolecular chains. The efficient photodegradation results in a significant reduction of the molecular weight in PEO as observed by Gel Permeation Chromatography or viscometric methods. The shorter chains formed after irradiation are more mobile and less entangled. In comparison to long chains, their motion and the regular packaging of degraded macromolecules is facilitated.

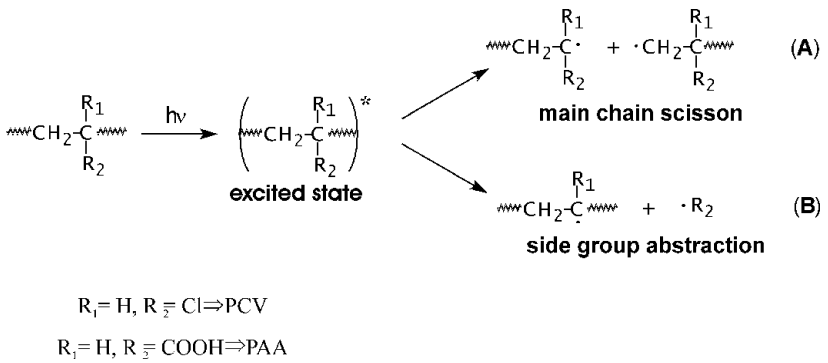

Scheme 2. The main reaction occurring in UV-irradiated polymers.

Furthermore, UV acts as an etching agent, that removes degradation products (such as simple organic compounds), usually enriched in the surface layer by evaporation. In this way, the very thin, amorphous surface layer is partially removed, and inner, compact spherulitic structures, come close to the surface and become visible in the optical microscope (Fig. 8). As can be seen, the spherulitic size decreases with irradiation time. This is also caused by chain scission, and the average diameter of spherulites is lower in UV-irradiated PEO.

Irradiated macromolecules are excited if they have absorbing groups. Although pure PEO should not absorb irradiation at a wavelength longer that 200 nm, it always contains impurities and structural defects, arising from production process (carbonyl and hydroperoxide groups, internal and end double bonds, residues of catalysts etc.) which can be directly excited. The properties of such excited macromolecules considerably differ from those which are not excited. They can change their conformations, which next changes lamellar order in spherulities. The development of these structures with increasing UV irradiation time is shown in Fig. 8.

3.3. Viscoelasticity measurements based on hysteresis loop assessment

In order to investigate the effect of UV radiation on sample visco-elasticity we performed indentation tests with repeated loading and unloading. These intelligent load functions result in multicycling indents at the same place on the sample surface. In Fig. 9(a) a typical time regime of the load function for multi-indentation is given. After loading, the force is decreased to 20% of the load maximum. This is done to avoid losing tip-to-sample contact. Then the sample is reloaded to a maximum force, which is 20% higher than that of the previous cycle. For samples, made of visco-elastic material, hysteresis loops [6,7] are observed (Fig. 9(b)). Hystersesis curves are observed in non-irradiated and UV radiated polymers. The convex shape of the unloading curves in Figs. 5 and 9 are the first hint for visco-elasticity in the polymer samples. The amount of visco-elasticity can be quantified by the area of the hysteresis loop. The larger the viscosity, the higher is the energy loss within a loading–unloading cycle [34]. In order to normalise the loop energy A it was divided by the purely elastically stored mechanical energy (area B below the entire unloading curve). The obtained results are presented in Table 1.

We found that for all polymers visco-elasticity decreases after UV irradiation. This means that they become stiffer, and a smaller amount of energy is transformed into heat. This effect is highest for PVC. The reduction in the visco-elastic properties are probably caused by photo-crosslinking in PVC and PAA, and by an increase of the crystalline fraction in irradiated PEO. In fact, the amount of insoluble gel exceeds 60% after 5 h UV irradiation in PVC, whereas photo-crosslinking is much less efficient in PAA. One can conclude, that the formation of a three-dimensional

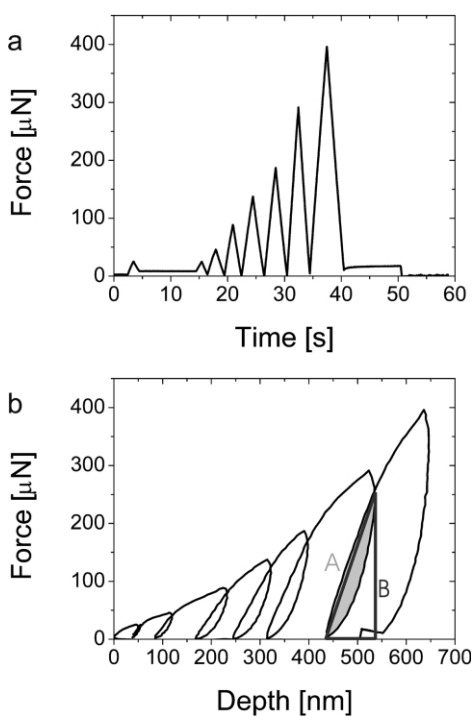

Fig. 9. Multi-indentation in non-irradiated PVC with an intelligent load function: (a) load-time function of the indentation regime and (b) the resulting force–depth curve with hysteresis loops. A quantification of the relative viscosity using the loading–reloading hysteresis and the extrapolated purely elastically stored mechanical energy is shown.

Table 1
Ratio of relative energy loss for polymers before and after UV exposition

	Relative energy loss (A/B)		
	PVC	PAA	PEO
Non-irradiated	0.5	0.35	0.43
Irradiated	0.25	0.29	0.31
Ratio	2.0	1.2	1.4

network, in which macromolecules have restrained mobility, is the reason for the decrease of dissipation energy after irradiation. The changes of crystallinity in UV-irradiated PEO do not have such a great influence on viscoelastic properties as photo-crosslinking in PVC or PAA.

4. Conclusions

The various calibration methods to establish a relation area—depth $A(h)$ resulted in very similar $A(h)$-functions. The small data scattering obtained for the same sample at different indentation depths confirmed the correctness of the used calibration. The nano-hardness measurements allows the study of the impact of photochemical reactions on mechanical properties of polymers with different structures.

UV irradiation causes an increase of hardness and indentation modulus in all samples: PEO, PVC and PAA. Moreover, a considerable loss of viscosity was observed in these samples when exposed to UV. The nanomechanical studies suggest that the crosslinking is a dominant reaction leading to a significant increase of the elastic indentation modulus and the nano-hardness and loss of viscoelasticity. In case of semicrystalline polymers like PEO, UV-induced rearrangements of molecules and the increase of the degree of the crystallinity are the main reasons for changes of mechanical properties measured on nanoscale.

Acknowledgements

This work was performed at the University of Applied Sciences Wildau within the framework of the International Quality Network project ‘Technology of New Materials’ (No 241) with financial support of the German Academic Exchange Service DAAD and the Future Investment Program in Germany ZIP. We gratefully acknowledge helpful discussion and critical reading of the manuscript by Roger Smith, Loughborough University, UK.

References

[1] Binnig G, Rohrer H. Helv Phys Acta 1982;55:726.
[2] Binnig G, Quate CF, Gerber C. Phys Rev Lett 1986;56:933.
[3] Magonov SN, Reneker DH. Annu Rev Mater Sci 1997;27:175.
[4] Goh MC. In: Prigogine I, Rice SA, editors. Advances in chemical physics, vol. XCI. Wiley; 1995.
[5] J Mater Res 1999;14(6). whole volume.
[6] Wolf B, Richter A. New J Phys 2003;5:15.1–15.17.
[7] Richter A, Wolf B, Smith R. Proceedings MRS spring meeting, San Francisco, USA. 2003.
[8] Maier P, Richter A, Faulkner RG, Ries R. Mater Character 2002;48:329–39.
[9] Murata H, Merrit CD, Inada H, Shrota Y, Zakaya HK. Appl Phys Lett 1999;21:3252.
[10] Capella G, Dietler G. Surf Sci 1999;34:1–104.
[11] Du B, Liu J, Zhang Q, He T. Polymer 2001;42:5901–7.
[12] Du B, Zhang J, Zhang Q, Yan D, He T, Tsui OK. Macromolecules 2000;33:7521–8.
[13] Drechsler D, Karbach A, Fuchs H. Appl Phys A 1998;66:825–9.
[14] Tanaka K, Takahara A, KajiYama T. Macromolecules 1998;31:5150–1.
[15] Tsui OK, Wang XP, Ho JYL, Ng TK, Xiao X. Macromolecules 2000;33:4198–204.
[16] Cahn RW, Haasen P, Kramer EJ, editors. Material science and technology, structure and properties of polymers, vol. 12. Weinhem: VCH; 1993.
[17] Ward IM, Hadley DW. An introduction to the mechanical properties of solid polymers. Chichester: Wiley; 1993.
[18] Rabek JF. Polymer photodegradation—mechanisms and experimental methods. London: Chapman & Hall; 1993.
[19] Rabek JF. Photodegradation of polymers. Physical characteristics and applications. Berlin: Springer Verlag; 1996.
[20] Zweifel H. Chimia 1993;10:390.
[21] Decker C. In: Cheremisinoff NP, editor. Handbook of polymer science and technology. Effect of UV radiation on polymers, vol. 3. New York: Marcel Dekker; 1989. p. 541.
[22] Olivier WC, Pharr GM. J Mater Res 1992;7:1562.
[23] Richter A, Ries R, Smith R, Henkel M, Wolf B. Diamond Relat Mater 2000;9:170–84.
[24] Thurn J, Cook RF. J Mater Res 2002;17:1143–6.
[25] www.vernay.com/corporate/elastomer.htm.
[26] www.goodfellow.com.
[27] Ohi A, Mizukani W, Tokumoto H. J Vac Sci Technol B 1995;13(3):1252–6.
[28] Wu K, Wisecarver KD. Biotechnol Bioeng 1992;39:447.
[29] Hen KC, Lin YF. Enzyme Microb Technol 1994;19:79.
[30] Ratnam CT. Polym-Plast Technol Engng 2002;41(3):407.
[31] Miranda T, Goncalves A, Amorim MT. Polym Int 2001;50:1068.
[32] Doytcheva M, Dotcheva D, Stemenov R, Tsvetanov C. Macromol Mater Engng 2001;286:30.
[33] Amitay-Sadowsky E, Ward B, Somorjai GA, Komvopoulos K. J Appl Phys 2002;91:375–81.
[34] Gilbert JL, Cumber J, Butterfield A. J Biomed Mater Res 2002;61:270–81.